A study of electron scattering from benzene: Excitation of the $^1B_{1u}$, $^3E_{2g}$, and $^1E_{1u}$ electronic states

Hidetoshi Kato,[1] Masamitsu Hoshino,[1] Hiroshi Tanaka,[1] Paulo Limão-Vieira,[2] Oddur Ingólfsson,[3] Laurence Campbell,[4] and Michael J. Brunger[5,a)]
[1]*Department of Physics, Sophia University, Chiyoda-ku, Tokyo 102-8554, Japan*
[2]*Laboratório de Colisões Atómicas e Moleculares, CEFITEC, Departamento de Física, FCT, Universidade Nova de Lisboa, 2829-516 Caparica, Portugal*
[3]*Department of Chemistry, Science Institute, University of Iceland, 107 Reykjavík, Iceland*
[4]*ARC Centre for Antimatter-Matter Studies, School of Chemical and Physical Sciences, Flinders University, GPO Box 2100, Adelaide, SA 5001, Australia*
[5]*Institute of Mathematical Sciences, University of Malaya, Kuala Lumpur 50603, Malaysia*

(Received 17 February 2011; accepted 21 March 2011; published online 7 April 2011)

We report results from measurements for differential and integral cross sections of the unresolved $^1B_{1u}$ and $^3E_{2g}$ electronic states and the $^1E_{1u}$ electronic state in benzene. The energy range of this work was 10–200 eV, while the angular range of the differential cross sections was ∼3°–130°. To the best of our knowledge there are no other corresponding theoretical or experimental data against which we can compare the present results. A generalized oscillator strength analysis was applied to our 100 and 200 eV differential cross section data, for both the $^1B_{1u}$ and $^1E_{1u}$ states, with optical oscillator strengths being derived in each case. The respective optical oscillator strengths were found to be consistent with many, but not all, of the earlier theoretical and experimental determinations. Finally, we present theoretical integral cross sections for both the $^1B_{1u}$ and $^1E_{1u}$ electronic states, as calculated within the BE*f*-scaling formalism, and compare them against relevant results from our measurements. From that comparison, an integral cross section for the optically forbidden $^3E_{2g}$ state is also derived. © *2011 American Institute of Physics*. [doi:10.1063/1.3575497]

I. INTRODUCTION

Benzene (C_6H_6), the simplest aromatic hydrocarbon, is a very important chemical compound due to its role as a key precursor in many synthetic processes employed by both the pharmaceutical and petrochemical industries. Indeed in many respects it can be thought of as the prototype aromatic system, displaying conjugative, delocalization, and resonance effects thereby making it an ideal system with which to study such phenomena. In addition, it also plays an important role in the chemistry of some planetary atmospheres including haze formation on Titan[1] and it has been found in the C-rich atmosphere of the protoplanetary nebula CRL618.[2] In chemistry, there has also been significant work (Refs. 3–5 and references therein) using benzene and its clusters, in order to study van der Waals interactions. Van der Waals clusters provide a means for the stepwise study of physical properties between a bare molecule and one completely solvated. They are thus very important if we want to obtain a fundamental understanding for the solvation process. Typically these studies involve using a pulsed UV laser as the probe and the velocity map imaging[3] technique to detect the resultant product ions. More recently,[6] benzene, in conjunction with a liquid microjet technique and coupled with laser spectroscopy, has also been used as a prototype species to study the evaporation process. From a scattering perspective, while benzene is a nonpolar molecule it possesses an extremely large polarizability (∼70 a.u.) so that one might anticipate its low-energy electron scattering dynamics to be dominated by polarization effects. It thus also represents an excellent prototype with which to study those effects. In addition while benzene is a relatively large molecule (42 electrons), it is highly symmetric making *ab initio* electron–polyatomic molecule scattering calculations more tractable than would otherwise be the case.

Considering its fundamental importance, it is thus somewhat surprising that studies investigating electron scattering from C_6H_6 are not particularly numerous. Experimental grand total cross sections, covering a fairly wide energy range, have been reported by several groups,[7–11] while dissociative excitation cross sections (30–1000 eV) were measured using a radiation emission technique by Beenakker and de Heer.[12] Elastic scattering cross section measurements have been made by Gulley and Buckman,[13] Cho *et al.*[14] Boechat–Roberty *et al.*,[15] and most recently from Sanches *et al.*[16] Relatively speaking, quite a few experimental investigations into vibrational excitation and resonance effects, at energies below 10 eV, have been published. These include the studies by Schulz and coworkers[17–20] and Mathur and Hasted.[21] Burrow *et al.*[22] determined the vertical electron affinities and characterized the temporary anion states of a series of hydrocarbons including benzene, using electron transmission spectroscopy, while a review of all these resonance studies was provided by Allan.[23] Most experimental studies into excitation of the $^1B_{1u}$ and

a)Electronic mail: Michael.Brunger@flinders.edu.au. Permanent address: ARC Centre for Antimatter-Matter Studies, School of Chemical and Physical Sciences, Flinders University, GPO Box 2100, Adelaide, SA 5001, Australia.

$^1E_{1u}$ electronic states have employed either photoabsorption or dipole (e,e′) techniques,[24–28] in order to determine their respective optical oscillator strengths (OOSs). Agreement between the various OOS measurements for the $^1E_{1u}$ state is typically very good to the ±5% level, however, for the $^1B_{1u}$ state there is a serious disagreement between the results of Feng *et al.*[24], and Suto *et al.*[25] on the one hand, and those of Philis *et al.*,[26] Pantos *et al.*[27] and Hammond and Price,[28] on the other. Finally, we note the total ionization cross section results from measurements due to Schram *et al.*[29]

From a theoretical perspective, elastic electron scattering from C_6H_6, at energies up to about 40 eV, using single-center expansion methods at the static exchange level, were reported by Gianturco and Lucchese.[30] Elastic data were also reported by Bettega *et al.*,[31] although in this case the Schwinger multichannel method at both the static exchange and static exchange plus polarization levels was utilized. Ma *et al.*,[32] using an independent atom model approach, reported elastic differential cross sections (DCSs), integral cross sections (ICSs) and momentum transfer cross sections for e^-–C_6H_6 scattering in the 100–1000 eV range. Similarly, different versions of the additivity rule have been applied in calculating total cross sections[33–35] for this scattering system. Theoretical optical oscillator strengths for the $^1E_{1u}$ electronic state have also been reported by several groups[36–41] with significant differences found between those results. As the theoretical OOS is an indication for the quality of the wavefunction used in a calculation, those differences therefore simply reflect the differing accuracy in the various wavefunctions used in those computations.[36–41]

In Sec. II of this paper we discuss our experimental details and analysis techniques. This is followed by a brief precis of our theoretical calculations in Sec. III before our results, and a discussion to those results are presented. Finally, some conclusions from the present investigation are drawn in Sec. V.

II. EXPERIMENTAL DETAILS AND ANALYSIS TECHNIQUES

The present spectrometer[42] consists of an electron gun with a hemispherical monochromator, a molecular beam crossed at right angles to the incident electrons, and a rotatable detector ($\theta = -10^\circ$ to 130°) with a second hemispherical analyzer system. A number of electron optic elements image and control the energy of the electron beam, with their performance having been checked by detailed electron trajectory calculations. Both the monochromator and analyzer are housed in differentially pumped boxes, in order to reduce the effect of any background gases and to minimize the stray electron background. The target molecular beam is produced by effusing C_6H_6 through a simple nozzle with an internal diameter of 0.3 mm and a length of 5 mm.

The incident electron energies (E_0) in the present study were 10, 15, 30, 100, and 200 eV, and the scattered electron angular range was $3.1^\circ-130^\circ$. In all of these cases the energy resolution was in the range 40−55 meV [full width at half maximum (FWHM)] and the angular resolution was $\sim \pm 1.5^\circ$ (FWHM). The primary electron beam current was typically

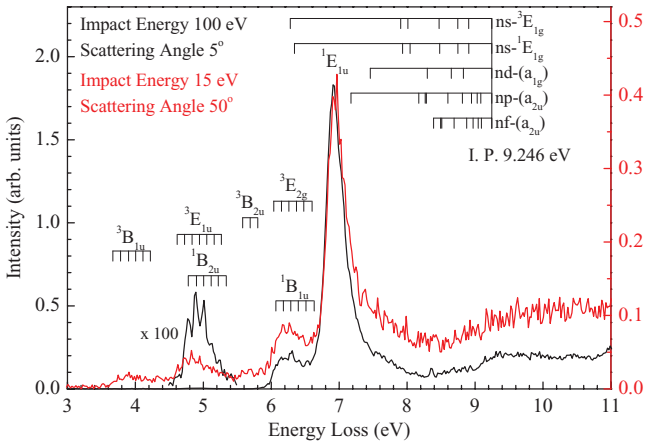

FIG. 1. Typical energy-loss spectra for electron impact excitation of the relevant electronic states in C_6H_6, at an impact energy of 15 and 100 eV and at a scattering angle of 50° and 5°, respectively.

in the range 3−8 nA. The incident electron energy was calibrated with respect to the 19.37 eV resonance of He.[43]

Electron energy loss spectroscopy (EELS) spectra were measured, at each incident electron energy and each scattered electron angle (θ). For the case of 10 eV incident electrons the energy loss was measured around the elastic peak and in the range from 3 to 9 eV. For all other incident energies the energy-loss range encompassed the elastic peak and the range from 3 to 11 eV. Typical examples of these data at $E_0 = 15$ eV and $\theta = 50^\circ$ and at $E_0 = 100$ eV and $\theta = 5^\circ$ are shown in Fig. 1. Note that in these figures we have deliberately omitted the elastic peak, in order to highlight the measured inelastic features. It is clear from these spectra that excitation of the $^1E_{1u}$ state dominates at both the kinematical conditions shown, although at 15 eV and 50° the $^1B_{1u} + {}^3E_{2g}$ excitation is relatively more significant due to an increased contribution from the $^3E_{2g}$ state. This we attribute to electron exchange becoming more important at the lower energies. The absolute scales on these EELS spectra were set using the relative flow technique[44] with helium elastic DCSs as the standard.[45] Note that for each of the $^1B_{1u} + {}^3E_{2g}$ and $^1E_{1u}$ electronic states this procedure sets their respective manifold DCSs, for the incident electron energy and electron scattering angle in question. For the incident energies of interest ($E_0 = 10-200$ eV) and the energy-loss range of interest ($\Delta E = 0-11$ eV or 0–9 eV), the ratio of the energy loss to the incident energy varies roughly in the range of $\sim 0 \leq \Delta E/E_0 \leq 0.9$. Thus, it is crucial to establish the transmission of the analyzer over this energy-loss range, with our procedure for doing so being found in Kato *et al.*[46] We also note the approach of Allan[47] in this regard.

Experimental errors on the present DCSs are estimated at about 18%−20%, including components due to the uncertainty in our analyzer transmission response, an uncertainty due to errors associated with the elastic normalization cross sections, and uncertainties due to any fluctuations in target density and/or the incident electron beam current during the measurements. The present experimental DCSs for the $^1B_{1u} + {}^3E_{2g}$ and $^1E_{1u}$ electronic states are plotted in Fig. 2

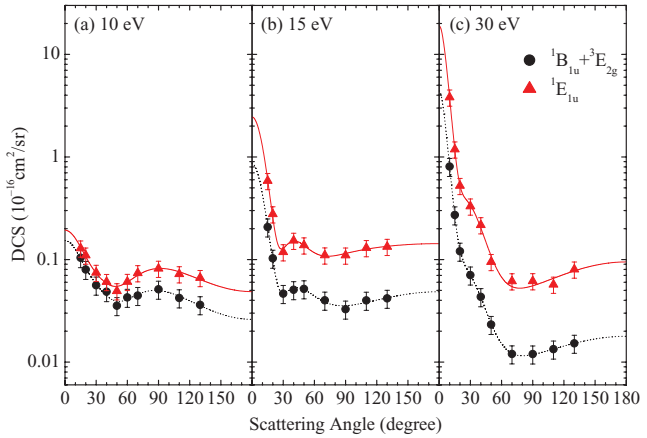

FIG. 2. The differential cross sections (10^{-16} cm^2/sr) for electron impact excitation of the $^1B_{1u} + {}^3E_{2g}$ and $^1E_{1u}$ electronic states in C_6H_6 at the incident electron energies (a) 10, (b) 15, and (c) 30 eV. See legend in the figure for further details. The solid and dashed lines in these figures are the results from applying our GOS fitting procedure, and subsequently converting them back to differential cross sections.

and tabulated in Tables I and II, with a full discussion of them being given later in Sec. IV of this paper.

The so-determined values of $[\theta, \mathrm{DCS}(\theta)]$, for each electronic state, are then transformed to (K^2, G_{expt}) using the standard formula[48]

$$G_{\mathrm{expt}}(K^2) = \frac{(E/R)k_i a_0}{4a_0^2 k_f a_0} K^2 \mathrm{DCS}(E_0, \theta), \tag{1}$$

TABLE I. Electron impact excitation DCSs (10^{-16} cm^2/sr) for the $^1B_{1u} + {}^3E_{2g}$ electronic states in C_6H_6. The estimated uncertainty in the DCS data is 20%.

Scattering angle (deg)	Impact energy (eV)				
	10	15	30	100	200
3.1					4.1422
3.3				5.8863	
4.7				2.9012	
4.9					1.1829
5.0				2.4929	
6.7				1.0523	
6.9					0.3422
8.7				0.4310	
8.9					0.1569
10.0			0.8067		
13.7				0.0997	
13.9					0.0454
15	0.1041	0.2073	0.2718		
20	0.0799	0.1028	0.1203		
30	0.0562	0.0465	0.0704		
40	0.0485	0.0507	0.0433		
50	0.0355	0.0517	0.0232		
60	0.0428				
70	0.0445	0.0401	0.0120		
90	0.0513	0.0328	0.0120		
110	0.0422	0.0400	0.0133		
130	0.0362	0.0418	0.0152		

TABLE II. Electron impact excitation DCSs (10^{-16} cm^2/sr) for the $^1E_{1u}$ electronic state in C_6H_6. The estimated uncertainty in the DCS data is 18%.

Scattering Angle (deg)	Impact energy (eV)				
	10	15	30	100	200
3.1					28.8426
3.3				42.1493	
4.7				19.8712	
4.9					7.4072
5.0				16.9343	
6.7				6.3175	
6.9					1.6921
8.7				2.4291	
8.9					0.5460
10.0			3.8135		
13.7				0.4673	
13.9					0.1819
15	0.1287	0.5852	1.1865		
20	0.1098	0.2771	0.5239		
30	0.0745	0.1183	0.3303		
40	0.0606	0.1529	0.2169		
50	0.0493	0.1379	0.0949		
60	0.0607				
70	0.0738	0.1101	0.0615		
90	0.0816	0.1098	0.0617		
110	0.0722	0.1298	0.0570		
130	0.0663	0.1333	0.0802		

where k_i and k_f are the initial and final momenta of the incident electron, a_0 is the Bohr radius (0.529 Å), R is the Rydberg energy (13.6 eV), E is the excitation energy for each electronic state, $G_{\mathrm{expt}}(K^2)$ is the experimental generalized oscillator strength (GOS), and K^2 is the momentum transfer squared defined by

$$K^2 = (k_i a_0)^2 + (k_f a_0)^2 - 2(k_i a_0)(k_f a_0)\cos\theta. \tag{2}$$

Vriens[49] proposed the following formula to represent the GOS for a dipole-allowed excitation, based on the analytic properties as identified by Lassettre[50] and Rau and Fano:[51]

$$G(x) = \frac{1}{(1+x)^6}\left[\sum_{m=0}^{\infty} \frac{f_m x^m}{(1+x)^m}\right], \tag{3}$$

where

$$x = \frac{K^2}{\alpha^2} \tag{4}$$

and

$$\alpha = \sqrt{\frac{B}{R}} + \sqrt{\frac{B-E}{R}} \tag{5}$$

with B being the binding energy of the target electron being excited. In Eq. (3) the f_m are fitting constants to be determined in a least-squares fit analysis of the experimental GOSs. The fitting results at 100 and 200 eV for each electronic state are shown in Fig. 3 where it can be seen that the quality of these fits is very good, as evidenced by a value of the fit correlation coefficient (r^2) of 0.98 for the $^1B_{1u}$ state and 0.99 for the $^1E_{1u}$ state. The experimental optical oscillator strengths can now be extracted from the f_0 coefficient that was determined

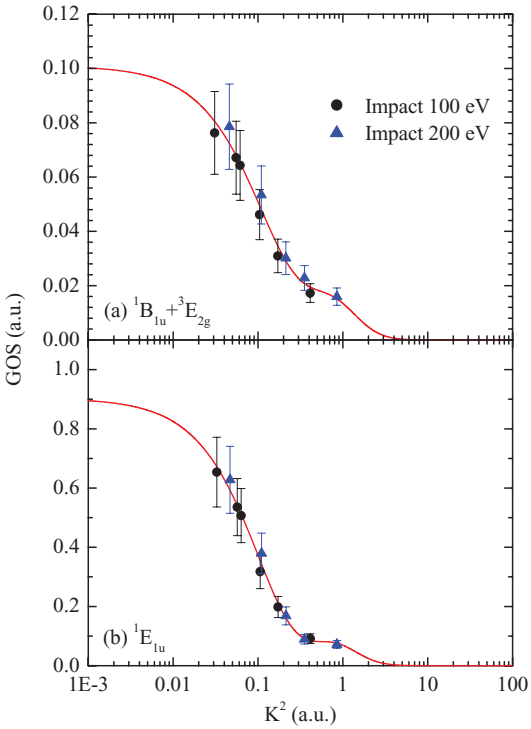

FIG. 3. Present GOS versus K^2 plots at 100 and 200 eV for the (a) $^1B_{1u}+^3E_{2g}$ and (b) $^1E_{1u}$ electronic states. The fits to the data (——) were performed using the formalism outlined in Sec. II of the paper. See legend in the figure for further details.

from the fit. Those values are listed in Table III, and also compared with previous experimental work[24–28] and theoretical work.[36–41] Note that in deriving an OOS for the $^1B_{1u}$ state we implicitly assume that any contribution from the optically-forbidden $^3E_{2g}$ will be small, and so can thus be neglected.

Finally, estimates of the ICS at each energy can be obtained from Eqs. (3)–(5) using the standard formulas[52]

$$\mathrm{ICS}(E_0) = \frac{4\pi a_0^2}{E_0/R}\int_{K^2_{\min}}^{K^2_{\max}} \frac{G(K^2)}{E/R} d\ln(K^2) \qquad (6)$$

TABLE III. A comparison between the present optical oscillator strengths and a selection of those from previous works (Refs. 24–28 and 36–41). The errors in the present OOSs are 20%.

Experiment	$^1B_{1u}$	$^1E_{1u}$
Present work	0.101	0.903
Feng (Ref. 24)	0.0312	0.824
Suto (Ref. 25)	0.03	0.84
Philis (Ref. 26)	0.090	0.900
Pantos (Ref. 27)	0.090	0.953
Hammond and Price (Ref. 28)	0.094	0.88
Theory		
Heinze (Ref. 36)		0.916
Chaudhuri (Ref. 37)		0.82
Hashimoto (Ref. 38)		0.76
Packer (Ref. 39)		0.51
Lorentzon (Ref. 40)		0.82
Kitao and Nakatsuji (Ref. 41)		1.03

TABLE IV. Present ICSs (10^{-16} cm^2) for electron impact excitation of the $^1B_{1u}+^3E_{2g}$ and $^1E_{1u}$ electronic states in C_6H_6. The estimated uncertainty in the ICSs data are 27% and 23%, respectively.

Impact energy (eV)	Integral cross section (10^{-16} cm^2)			
	BEf-scaled ($^1B_{1u}$)	Present work ($^1B_{1u}+^3E_{2g}$)	BEf-scaled ($^1E_{1u}$)	Present work ($^1E_{1u}$)
6.19	0.0000			
6.2	0.0057			
6.4	0.0276			
6.6	0.0405			
6.96			0.0000	
7.0	0.0614			
7.5	0.0838		0.2487	
8.0	0.1037		0.3882	
8.5	0.1217		0.5154	
9.0	0.1380		0.6341	
9.5	0.1529		0.7451	
10	0.1666	0.5651	0.8492	0.8906
15	0.2549	0.6354	1.5808	1.8898
20	0.2940		1.9510	
30	0.3152	0.5100	2.2204	2.3808
40	0.3099		2.2456	
50	0.2969		2.1890	
60	0.2821		2.1049	
70	0.2675		2.0140	
80	0.2539		1.9244	
90	0.2414		1.8394	
100	0.2299	0.2787	1.7600	1.8124
150	0.1860		1.4446	
200	0.1576	0.1991	1.2329	1.2693
300	0.1215		0.9593	
400	0.1006		0.7972	
500	0.0861		0.6841	
600	0.0764		0.6071	
700	0.0693		0.5499	
800	0.0630		0.5005	
900	0.0589		0.4662	
1000	0.0547		0.4331	
1500	0.0445		0.3463	
2000	0.0409		0.3115	

with

$$K^2_{\min} = 2\frac{E_0}{R}\left[1 - \frac{E}{2E_0} - \sqrt{1 - \frac{E}{E_0}}\right] \qquad (7)$$

and

$$K^2_{\max} = 2\frac{E_0}{R}\left[1 - \frac{E}{2E_0} + \sqrt{1 - \frac{E}{E_0}}\right]. \qquad (8)$$

The results from this latter process are listed in Table IV and plotted in Figs. 4 and 5.

III. THEORY

A full description of the BEf-scaling approach that we have employed here, to calculate ICSs for the $^1B_{1u}$ and $^1E_{1u}$ states, can be found in Kim,[48] so that only a brief discussion of the more important details need be given here. Note that the scaled (plane wave) Born cross sections that we used in

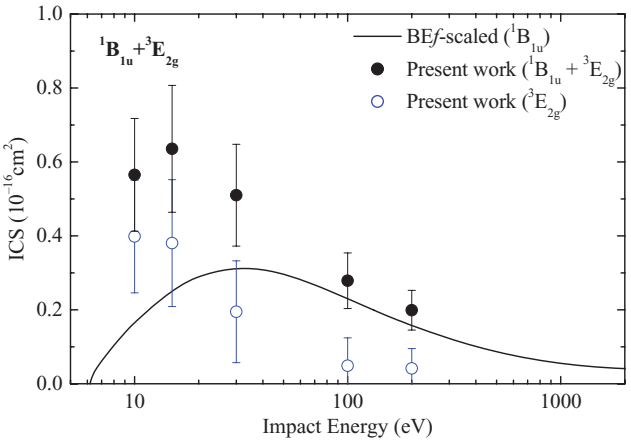

FIG. 4. The integral cross sections (10^{-16} cm^2) for electron impact excitation of the $^1B_{1u}+^3E_{2g}$ electronic states in C_6H_6. See legend in the figure and text for further details.

conjunction with this technique are not only subject to the approximations in the collision theory part, but also depend on the accuracy of the wavefunctions used for the initial and final states of the target molecule.

The f-scaled Born cross sections (ICS_f) are given by

$$ICS_f(E_0) = \frac{f_{accur}}{f_{Born}} ICS_{Born}(E_0), \quad (9)$$

where f_{accur} is an accurate OOS value from either accurate wavefunctions or experiments and f_{Born} is the OOS from the same wavefunctions used to calculate the unscaled Born cross sections $ICS_{Born}(E_0)$. The f-scaling process has the effect of replacing poor or marginal wavefunctions with something more physical. We note that the ICS_{Born} for the $^1B_{1u}$ and $^1E_{1u}$ states were taken from Read and Whiterod,[53] and accurate OOSs were taken from Pantos *et al.*[27] which were recommended by Berkowitz.[54]

The BE-scaled Born cross section (ICS_{BE}) is given by

$$ICS_{BE}(E_0) = \frac{E_0}{(E_0 + B + E)} ICS_{Born}(E_0). \quad (10)$$

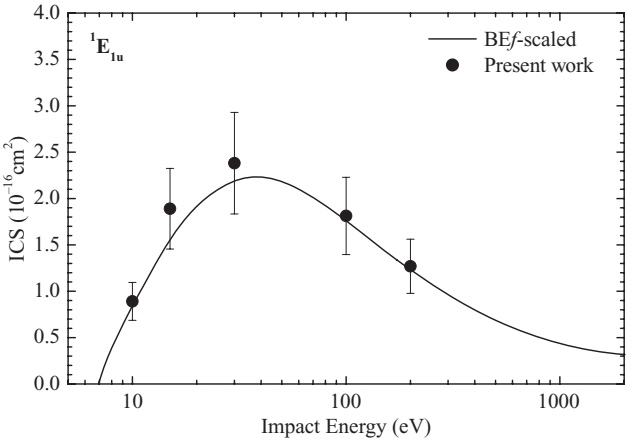

FIG. 5. The integral cross sections (10^{-16} cm^2) for electron impact excitation of the $^1E_{1u}$ electronic state in C_6H_6. See legend in the figure for further details.

This scaling corrects the well-known deficiency of the Born approximation at low E_0, without losing its established validity at high E_0.

If an unscaled $ICS_{BE}(E_0)$ is obtained from poor or marginal wavefunctions while an accurate OOS is known, then both f-scaling and BE-scaling can be applied to obtain a BE f-scaled Born cross section [$ICS_{BEf}(E_0)$]

$$ICS_{BEf}(E_0) = \frac{f_{accur}}{f_{Born}} \frac{E_0}{E_0 + B + E} ICS_{Born}(E_0). \quad (11)$$

The current calculated $ICS_{BEf}(E_0)$ are listed for the $^1B_{1u}$ and $^1E_{1u}$ states in Table IV. We also compare our experimental ICS and BE f-scaled Born cross sections in Figs. 4 and 5.

IV. RESULTS AND DISCUSSION

In Tables I and II we list our measured DCSs for the electron impact excitation of the $^1B_{1u}+^3E_{2g}$ and $^1E_{1u}$ electronic states. Our estimated errors on the $^1B_{1u}+^3E_{2g}$ cross sections are ~20%, while those for the $^1E_{1u}$ cross sections are ~18%. All these cited errors are at the one standard deviation level. A selection of the present data, for both the unresolved $^1B_{1u}$ and $^3E_{2g}$ states and the $^1E_{1u}$ state, are also plotted in Fig. 2. It should be immediately clear from this figure that there are no other theoretical and experimental data against which we can compare the present results. Nonetheless, we are still able to make some general observations regarding the behavior of our measured DCSs. First, all the present cross sections are forward peaked in magnitude as you go to smaller scattered electron angles. Furthermore, the degree of this forward peaking increases significantly as you go to higher incident electron energies. We believe these observations can be explained by the long-range, direct scattering, interaction between the incident electron and the extended charge cloud of the benzene molecule, as indicated by benzene's very large polarizability. There is a suggestion, particularly at the lower energies, of some structure in the angular distributions for both the $^1B_{1u}+^3E_{2g}$ and $^1E_{1u}$ states. This is likely to be caused by constructive and destructive interference effects between the partial waves describing the scattering process at these energies. However, we cannot rule it out being due to a resonant decay into those states. In this latter respect an excitation function measurement (i.e., DCS versus energy at a fixed scattering angle, e.g., 90°) for both electronic states would be interesting and would certainly help clarify matters. Finally, we also believe that the angular distributions in Fig. 2 reflect the important role that electron exchange plays at lower incident electron energies. This is manifested through the increased contribution in the excitation of the $^3E_{2g}$ state. For example, if we consider the $\theta_e = 110°$ cross sections at 10, 15, and 30 eV, then at 10 eV the $^1E_{1u}$ DCS is a factor of only ~1.7 times greater than the $^1B_{1u}+^3E_{2g}$ value, while at 20 eV it is a factor of ~3.2 times greater and finally at 30 eV it is a factor of ~4.3 times greater. This shows that as the incident electron energy is increased the relative population into the $^3E_{2g}$ state due to electron exchange declines in magnitude.

Applying the GOS versus K^2 analysis procedure we outlined in Sec. II, to our 100 and 200 eV $^1B_{1u}+^3E_{2g}$ and $^1E_{1u}$ DCSs, we are able to determine OOSs for the $^1B_{1u}$ electronic

state and the $^1E_{1u}$ electronic state. For the $^1B_{1u}$ state we can assume that at these energies the $DCS_{^3E_{2g}} \lll DCS_{^1B_{1u}}$ and so the $^3E_{2g}$ contribution can be ignored. The high-quality fits we achieved are illustrated in Fig. 3, while the so-determined OOSs are listed in Table III along with the results from previous experimental[24–28] and theoretical[36–41] investigations. Note that we estimate the uncertainty, again at the one standard deviation level, on our OOSs to be ∼20%. For the $^1E_{1u}$ electronic state, the present OOS is in very good agreement, to within our stated uncertainty, with all the previous experimental determinations[24–28] and some of the corresponding theoretical results.[36,37,40,41] For the $^1B_{1u}$ state, however, while we are in very good agreement with the OOS data of Philis *et al.*,[26] Pantos *et al.*,[27] and Hammond and Price,[28] all these authors and the present are approximately three times larger than the OOS from Feng *et al.*[24] and Suto *et al.*[25] We believe that the present measurements now confirm the OOSs for the $^1E_{1u}$ and $^1B_{1u}$ states, effectively benchmarking them for theory to test against the quality of their wavefunctions. Lewis[55] had previously suggested that the energies 100 and 200 eV might be too low in value in order to determine an accurate value of the OOS for the state in question, with the OOS determined at such energies being smaller than the physical or correct result. However, Table III clearly shows the present OOS values are in the upper range of all those determined. Hence we believe the point of Lewis[55] is probably not general, rather it is species specific.

In Table IV and Figs. 4 and 5 we present our experimental integral cross section results for the electron impact excitation of the $^1B_{1u}+^3E_{2g}$ and $^1E_{1u}$ electronic states. The uncertainty on those data is ∼ ±27% and ±23%, respectively. Also included in that table and those figures are the results of our BE*f*-scaling calculations for the $^1B_{1u}$ and $^1E_{1u}$ states from their thresholds up to 2000 eV. Considering first Fig. 5, we find a truly remarkable level of accord between our experimental ICSs and those from the BE*f*-scaling technique, over the common energy range of comparison. Benzene is by far the largest molecule we have yet considered in our studies[46,56–61] seeking to investigate the efficacy of the BE*f*-scaling approach, in particular in relation to providing reliable data bases for the plasma modeling community. Thus, the level of agreement seen in Fig. 5 is heartening, and consistent with what we have observed previously[46,56–61] for other species when resonance (i.e., the decay of a temporary negative (anion) state into the channel in question) effects are not apparent and when strong Rydberg-valence interactions are absent. With respect to Fig. 4, we see good agreement between the present BE*f*-scaling result for the $^1B_{1u}$ state and the measured data for energies greater than 100 eV. This occurs because above 100 eV, the contribution from the $^3E_{2g}$ state to the measured data must be small. At energies lower than 100 eV, however, the measured ICSs are significantly higher than those from our BE*f*-scaling results. This reflects the increasing $^3E_{2g}$ contribution to the measured ICSs as the effect of electron exchange becomes more important. We noted above that there are many examples,[46,56–61] for dipole-allowed transitions, where the BE*f*-scaling approach provides a very realistic description of the ICS for that excitation process. As a consequence we have subtracted the BE*f*-scaling ICSs for the $^1B_{1u}$ state from our measured $^1B_{1u}+^3E_{2g}$ ICSs, in order to determine the ICSs for the optically-forbidden $^3E_{2g}$ electronic state. The results of this process can also be found in Fig. 4 (open circles). Hence, it appears that if an optically allowed transition serendipitously overlays with an optically forbidden transition (i.e., singlet → triplet in this case), we now have a procedure by which the integral cross sections for that optically forbidden transition can be extracted. This, thus, represents an alternative way to increase the available cross section data base for a given molecule.

V. CONCLUSIONS

We have reported on a comprehensive investigation into electron impact excitation of the $^1B_{1u}$, $^3E_{2g}$, and $^1E_{1u}$ electronic states in benzene. The present $^1B_{1u}+^3E_{2g}$ and $^1E_{1u}$ differential cross sections are original, we know of no other experimental or theoretical results against which we could compare them. The effect of the very large long-range dipole polarizability on the scattering dynamics of these systems was apparent in both cases, while the effect of exchange, on the $^1B_{1u} + ^3E_{2g}$ angular distributions, was also observed at incident electron energies closer to their excitation thresholds. This was of course due to the excitation of the $^3E_{2g}$ state from benzene's singlet ground ($X\ ^1A_{1g}$) electronic state. Optical oscillator strengths from this study for both the $^1B_{1u}$ and $^1E_{1u}$ electronic states were in most cases in good agreement with the results from previous measurements, thereby benchmarking those states for theoreticians wishing to test the accuracy of the wavefunctions they respectively use to represent them. Experimental integral cross sections for the $^1B_{1u} + ^3E_{2g}$ and $^1E_{1u}$ states were also reported, and in this case compared against theoretical results from our application of the BE*f*-scaling approach for the $^1B_{1u}$ and $^1E_{1u}$ states. Agreement between our measured ICS and those from the BE*f*-scaling method for the $^1E_{1u}$ state was excellent, across the entire common energy range. Assuming a similar level of accord for the $^1B_{1u}$ state, and we presented strong evidence for why this might be the case, an ICS for the $^3E_{2g}$ state was determined. This $^3E_{2g}$ ICS exhibited all the features we might *a priori* expect for a singlet → triplet excitation. Namely, a strong increase in its magnitude for energies from threshold (E_{th}) until a maximum is reached at an energy of $\sim 2E_{th}$. Thereafter, the magnitude of the $^3E_{2g}$ electronic state ICSs monotonically decreased in value with increasing incident electron energy, until at about 100 eV it becomes so small that it can virtually be neglected. This ability to use measured ICS data in conjunction with the BE*f*-scaling approach for dipole-allowed transitions, in order to extract ICS for optically forbidden states, is potentially of great utility for workers seeking to establish complete data sets for plasma, atmospheric, or biomedical modeling applications.

ACKNOWLEDGMENTS

This work was conducted under the support of the Japanese Ministry of Education, Sport, Culture and Technology. Additional support from the Australian Research

Council, through its Centres of Excellence Programme, and RANNIS in Iceland is further noted. One of us (P.L.-V.) acknowledges his Visiting Professor position at Sophia University, Tokyo, Japan. This work also forms part of the EU COST Actions CM0601 and CM0805 programs. Finally, M.J.B. thanks the University of Malaya for providing him the Distinguished Visiting Professor position in the university.

[1]E. H. Wilson, S. K. Atreya, and A. Coustenis, J. Geophys. Res. **108**, 5014, doi:10.1029/2002JE001896 (2003).
[2]J. Cernicharo, A. M. Heras, A. G. G. M. Tielens, J. R. Pardo, F. Herpin, M. Guélin, and L. B. F. M. Waters, Astrophys. J. **546**, L123 (2001).
[3]J. R. Gascooke and W. D. Lawrance, J. Phys. Chem. A **104**, 10328 (2000).
[4]R. K. Sampson and W. D. Lawrance, Aust. J. Chem. **56**, 275 (2003).
[5]E. R. Waclawik and W. D. Lawrance, J. Phys. Chem. A **107**, 10507 (2003).
[6]O. J. Maselli, J. R. Gascooke, W. D. Lawrance, and M. A. Buntine, J. Phys. Chem. C **113**, 637 (2009).
[7]W. Holst and J. Holtsmark, Forh. -K. Nor. Vidensk. Selsk. **4**, 89 (1931).
[8]O. Sueoka, J. Phys. B **21**, L631 (1988).
[9]P. Możejko, G. Kasperski, C. Szmytkowski, G. P. Karwasz, R. S. Brusa, and A. Zecca, Chem. Phys. Lett. **257**, 309 (1996).
[10]R. J. Gulley, S. L. Lunt, J.-P. Ziesel, and D. Field, J. Phys. B **31**, 2735 (1998).
[11]C. Makochekanwa, O. Sueoka, and M. Kimura, Phys. Rev. A **68**, 032707 (2003).
[12]C. I. M. Beenakker and F. J. de Heer, Chem. Phys. Lett. **29**, 89 (1974).
[13]R. J. Gulley and S. J. Buckman, J. Phys. B **32**, L405 (1999).
[14]H. Cho, R. J. Gulley, K. Sunohara, M. Kitajima, L. J. Uhlmann, H. Tanaka, and S. J. Buckman, J. Phys. B **34**, 1019 (2001).
[15]H. M. Boechat-Roberty, M. L. M. Rocco, C. A. Lucas, and G. G. B. de Souza, J. Phys. B **37**, 1467 (2004).
[16]I. P. Sanches, R. T. Sugohara, L. Rosani, M.-T. Lee, and I. Iga, J. Phys. B **41**, 185202 (2008).
[17]L. Sanche and G. J. Schulz, J. Chem. Phys. **58**, 479 (1973).
[18]I. Nenner and G. J. Schulz, J. Chem. Phys. **62**, 1747 (1975).
[19]R. Azria and G. J. Schulz, J. Chem. Phys. **62**, 573 (1975).
[20]S. F. Wong and G. J. Schulz, Phys. Rev. Lett. **35**, 1429 (1975).
[21]D. Mathur and J. B. Hasted, J. Phys. B **9**, L31 (1976).
[22]P. D. Burrow, J. A. Michejda, and K. D. Jordan, J. Chem. Phys. **86**, 9 (1987).
[23]M. Allan, J. Electron Spectrosc. Relat. Phenom. **48**, 219 (1989).
[24]R. Feng, G. Cooper, and C. E. Brion, J. Electron Spectrosc. Relat. Phenom. **123**, 199 (2002).
[25]M. Suto, X. Wang, J. Shan, and L. C. Lee, J. Quant. Spectrosc. Radiat. Transf. **48**, 79 (1992).
[26]J. Philis, A. Bolovinos, G. Andritsopoulos, E. Pantos, and P. Tsekeris, J. Phys. B **14**, 3621 (1981).
[27]E. Pantos, J. Philis, and A. Bolovinos, J. Mol. Spectrosc. **72**, 36 (1978).
[28]V. J. Hammond and W. C. Price, Trans. Faraday Soc. **51**, 605 (1955).
[29]B. L. Schram, M. J. van der Wiel, F. J. de Heer, and H. R. Moustafa, J. Chem. Phys. **44**, 49 (1966).
[30]F. A. Gianturco and R. R. Lucchese, J. Chem. Phys. **108**, 6144 (1998).
[31]M. H. F. Bettega, C. Winstead, and V. McKoy, J. Chem. Phys. **112**, 8806 (2000).
[32]E.-J. Ma, Y.-G. Ma, X.-Z. Cai, D.-Q. Fang, W.-Q. Shen, and W.-D. Tian, Chin. Phys. Lett. **25**, 97 (2008).
[33]D. Shi, J. Sun, Y. Liu, and Z. Zhu, J. Phys. B **41**, 025205 (2008).
[34]F. Blanco and G. Garcia, Phys. Lett. A **317**, 458 (2003).
[35]F. Blanco and G. Garcia, Phys. Lett A **360**, 707 (2007).
[36]H. H. Heinze, A. Görling, and N. Rösch, J. Chem. Phys. **113**, 2088 (2000).
[37]R. K. Chaudhuri, A. Mudholkar, K. F. Freed, C. H. Martin, and H. Sun, J. Chem. Phys. **106**, 9252 (1997).
[38]T. Hashimoto, H. Nakano, and K. Hirao, J. Chem. Phys. **104**, 6244 (1996).
[39]M. J. Packer, E. K. Dalskov, T. Enevoldsen, H. J. A. Jensen, and J. Oddershede, J. Chem. Phys. **105**, 5886 (1996).
[40]J. Lorentzon, P.-A. Malmqvist, M. Fülscher, and B. O. Roos, Theor. Chim. Acta **91**, 91 (1995).
[41]O. Kitao and H. Nakatsuji, J. Chem. Phys. **87**, 1169 (1987).
[42]H. Tanaka, T. Ishikawa, T. Masai, T. Sagara, L. Boesten, M. Takekawa, Y. Itikawa, and M. Kimura, Phys. Rev. A **57**, 1798 (1998).
[43]J. N. H. Brunt, G. C. King, and F. H. Read, J. Phys. B **10**, 1289 (1977).
[44]S. K. Srivastava, A. Chutjian, and S. Trajmar, J. Chem. Phys. **63**, 2659 (1975).
[45]L. Boesten and H. Tanaka, At. Data Nucl. Data Tables **52**, 25 (1992).
[46]H. Kato, H. Kawahara, M. Hoshino, H. Tanaka, M. J. Brunger, and Y.-K. Kim, J. Chem. Phys. **126**, 064307 (2007).
[47]M. Allan, J. Phys. B **38**, 3655 (2005).
[48]Y.-K. Kim, J. Chem. Phys. **126**, 064305 (2007).
[49]L. Vriens, Phys. Rev. **160**, 100 (1967).
[50]E. N. Lassettre, J. Chem. Phys. **43**, 4479 (1965).
[51]A. R. P. Rau and U. Fano, Phys. Rev. **162**, 68 (1967).
[52]B. H. Bransden and C. J. Joachain, *Physics of Atoms and Molecules* (Longman, London, 1983).
[53]F. H. Read and G. L. Whiterod, Proc. Phys. Soc. London **85**, 71 (1965).
[54]J. Berkowitz, *Atomic and Molecular Photoabsorption: Absolute Total Cross Sections* (Academic, San Diego, 2002).
[55]B. R. Lewis, Phys. Rev. A **78**, 026701 (2008).
[56]P. A. Thorn, M. J. Brunger, P. J. O. Teubner, N. Diakomichalis, T. Maddern, M. A. Bolorizadeh, W. R. Newell, H. Kato, M. Hoshino, H. Tanaka, H. Cho, and Y.-K. Kim, J. Chem. Phys. **126**, 064306 (2007).
[57]H. Kawahara, H. Kato, M. Hoshino, H. Tanaka, and M. J. Brunger, Phys. Rev. A **77**, 012713 (2008).
[58]H. Kawahara, H. Kato, M. Hoshino, H. Tanaka, L. Campbell, and M. J. Brunger, J. Phys. B **41**, 085203 (2008).
[59]H. Kato, H. Kawahara, M. Hoshino, H. Tanaka, L. Campbell, and M. J. Brunger, Phys. Rev. A **77**, 062708 (2008).
[60]H. Kawahara, D. Suzuki, H. Kato, M. Hoshino, H. Tanaka, O. Ingólfsson, L. Campbell, and M. J. Brunger, J. Chem. Phys. **131**, 114307 (2009).
[61]D. Suzuki, H. Kato, M. Ohkawa, K. Anzai, H. Tanaka, P. Limão-Vieira, L. Campbell, and M. J. Brunger, J. Chem. Phys. **134**, 064311 (2011).